Steel and Composite Structures, *Vol. 24, No. 2 (2017) 249-264*
DOI: https://doi.org/10.12989/scs.2017.24.2.249

Investigation of the vibration of lattice composite conical shells formed by geodesic helical ribs

Reza Nezamoleslami [a] and Siamak E. Khadem*

Department of Mechanical Engineering, Tarbiat Modares University, Tehran, Iran,
P.O. Box 14115-177, Tehran, Islamic Republic of Iran

(*Received June 04, 2016, Revised February 15, 2017, Accepted March 25, 2017*)

Abstract. In this paper free linear vibration of lattice composite conical shells will be investigated. Lattice composite conical shell consists of composite helical ribs and thin outer skin. A smeared method is employed to obtain the variable coefficients of stiffness of conical shell. The ribs are modeled as a beam and in addition to the axial loads, endure shear loads and bending moments. Therefore, theoretical formulations are based on first-order shear deformation theory of shell. For verification of the obtained results, comparison is made with those available in open literature. Also, using FEM software the 3D finite element model of composite lattice conical shell is built and analyzed. Comparing results of analytical and numerical analyses show a good agreement between them. Some special cases as variation of geometric parameters of lattice part, effect of the boundary conditions and influence of the circumferential wave numbers on the natural frequencies of the conical shell are studied. It is concluded, when mass and the geometrical ratio of the composite lattice conical shell do not change, increment the semi vertex angle of cone leads to increase the natural frequencies. Moreover for shell thicknesses greater than a specific value, the presence of the lattice structure has not significant effect on the natural frequencies. The obtained results have novelty and can be used for further and future researches.

Keywords: conical shell; lattice; composite; helical rib; smear method; shear deformation

1. Introduction

The practical importance of vibration analysis of conical shells, i.e. frequencies and mode shapes has been increased in structural, aerospace, chemical, submarine hulls, and mechanical applications. Thus, it is necessary for design engineers to evaluate the dynamic characteristics of this type shell structures effectively and accurately. A number of analytical and numerical studies have been conducted on the free vibration analysis of conical shells. For example the general dynamical behavior of conical shells has been investigated by Saunders *et al*. (1960) and Garnet and Kempner (1960). A transfer-matrix approach for free vibration of conical shells with constant and variable thickness developed by Irie *et al*. (1982, 1984). Using the finite element method Sivadas and Ganesan (1992) analyzed the free vibration of conical shells with uniform thickness. Yang (1974) adopted the integration method in the vibration analysis of orthotropic conical shells. Siu and Bert (1970) presented free vibration of conical shells by using the Ritz technique. Tong (1993a, b, 1994) examined the vibration analysis of isotropic, orthotropic and laminated conical shells by the power series expansion method. Recently, Liew and Lim (1995) and (Liew *et al*. 1997) presented the differential quadrature method to study the free vibration of orthotropic and laminated conical shells. Lim and Liew (1995) also studied the vibration behavior of shallow shells via Ritz method. Some selected works in this research topic includes those of Chang (1981), Shu (1996), Liew *et al*. (1995), Civalek (2006a, b, 2007, 2008, 2013), Lim *et al*. (1998) and Liew *et al*. (2005), Sofiyev and Karaca (2009), Sofiev *et al*. (2009) and Sofiyev and Kuruoglu (2011). Bakshi and Chakravorty (2013) using Lagrange's equation of motion in conjunction with Hamilton's principle and a finite element code studied static bending, free and forced vibration responses of composite conoidal shells. Although, vibration analysis of orthotropic composite shell structures with different geometries like cylinders and cones have been investigated by many researchers, the subject of the vibrational behavior of composite lattice shells and specially conical ones has received very little attention in the scientific literature until recently. Lattice composite structures do not have any analogues in cost and weight efficiency so they could compete in the class of high-loaded structures. Considering industrial applications of lattice structures, the dynamical behavior of these structures very important and need to be investigated. Although lattice composite conical shells beside the cylindrical ones, due to their unique specifications are used in various structural applications as aerospace engineering such as fairings and payload adapters for spacecraft launchers as studied Vasiliev *et al*. (2001) and Vasiliev and Rasin (2006), most of these studies about lattice structures dedicated to static analysis and determine stress and stability or investigation of buckling and also

*Corresponding author, Professor,
E-mail: Khadem@modares.ac.ir
[a] Ph.D. Student, E-mail: R.Nez.El@gmail.com

ISSN: 1229-9367 (Print), 1598-6233 (Online)

fabrication and testing of these shells and mainly related to composite lattice cylindrical shells. Gürdal and Gendron (1993) based on finite element method designed optimum geodesically grid-stiffened cylindrical shells respect to weight. Thickness of plies and orientations of the skin laminate and stiffener heights were used as design variables. Kim (1999, 2000) investigated fabrication and testing of isogrid stiffened cylinder and composite stiffened panel, Slinchenko and Verijenko (2001) presented an analysis of cylindrical isogrid lattice shells, using an equivalent stiffness smearing method. Kidane *et al*. (2003) studied global buckling load for a generally cross and horizontal grid stiffened composite cylinder and developed an analytical model for determination of the equivalent stiffness parameters of a grid stiffened composite cylindrical shell. Wodesenbet *et al*. (2003) investigated the buckling problem of an isogrid stiffened composite cylinder developing an improved smeared method. Totaro and Gürdal (2005, 2009) studied optimal design of composite lattice structures for Aerospace application and developed an optimization method for composite lattice shell structures under axially compressive loads. Totaro (2012) investigated a refined analytical model for the local buckling failure modes of composite anisogrid lattice cylindrical shells made of a regular system of triangular cells. Totaro and De Nicola (2012) studied recent advance on design and manufacturing of composite anisogrid structures for space launchers. Also Totaro (2013b) and Totaro (2013a) theoretical studied local buckling modeling of isogrid and anisogrid lattice cylindrical shells with hexagonal cells and by experiment investigated the theoretical results. Buragohain and Velmurugan (2011) carried out axial compression tests for filament wound grid-stiffened composite cylindrical structures and compared results with finite element analysis. Morozov *et al*. (2011a, b) investigates the buckling behaviour of anisogrid composite lattice cylindrical shells under axial compression using the finite-element software package COSMOS/M . Recently Shi *et al*. (2013) studied critical local and global buckling loads of grid-stiffened carbon-fiber conical shells. The listed above scientific papers are associated with static study of composite lattice structures and mainly consider the cylindrical shells. In the field of dynamic studies of composite lattice structures, the number of scientific papers is insignificant. Golfman (2007) investigated dynamic stability of lattice cylindrical shell made of carbon fiber epoxy composites. Considering free and force vibration of lattice cylinder, He took into account damping properties of structure. Liang *et al*. (2011) numerically investigated the buckling and dynamic analysis of composite grid-stiffened cylindrical structure. Using a four node hybrid stress finite element Darilmaz (2012) studied stiffened orthotropic corner supported hypar shells and examined the influence of stiffener location, rise/span ratio and fiber orientation on vibration behavior of these shells. Hemmatnezhad *et al*. (2014) analytically investigated the vibrational behavior of grid-stiffened composite cylindrical shells and verified the obtained results by a 3-D finite element model using ABAQUS CAE software. Morozov *et al*. (Lopatin *et al*. 2015, 2016), using the semi-membrane theory of ortho-tropic cylindrical shells and finite element method studied free vibrations of a cantilever and clamped composite lattice cylindrical shell. The filament-wound lattice cylinders are modelled as a continuous shell characterized by the effective stiffness parameters. Recently Ansari and Torabi (2016), numerically studied the buckling and vibration of functionally graded carbon nanotube-reinforced composite conical shells under axial loading. He derived the governing equations using Hamilton's principle on the basis of the first order shear deformation theory.

It is clear that the listed above studies about vibrational behavior of the lattice structures although small in quantity, mainly related to cylindrical lattice shells. So, investigation of the dynamical behavior of lattice composite conical shells is novel and can be used for further and future researches.

2. Geometrical relationships for conical lattice shells

Conical Anisogrid (anisotropic grid) composite structures are specific lattice shells which are made by geodesic winding, like the cylindrical shells. Nevertheless, because of the geometrical properties of the conical surface, the corresponding geodesic trajectories are more complicated than those that are typical for the cylindrical lattice structures. In the conical shells, the helical angle (with respect to the local meridian of the shell) is continuously changing from the top to the bottom of the structure. As a consequence, the equations for the structural mass, stiffness and stresses are more complicated than those for the cylindrical structure. The conical lattice shell is characterized by variable properties which changes along the axis (Totaro 2011). Supposing geometrical differences between conical and cylindrical lattice shells, it is implicit that despite of cylindrical shell in which filament angle of grids, radius of and distances between helical and hoop ribs are constant, in conical shells these parameters are non-constant and variable with respect to variable radius of conical lattice shell. Since these parameters affect the coefficients of stiffness of lattice conical shell, one needs to consider them. Considering Fig. 1(a) and Fig. 2, these parameters are as follow (Totaro and Gürdal 2009)

$$\begin{aligned} &\phi_1 = \arctan\left(\frac{R_2 \sin(\gamma)}{R_2 \cos(\gamma) - R_1}\right), \phi_2 = \phi_1 - \gamma, \\ &\phi = \arcsin\left(\frac{R_1 \sin(\phi_1)}{R}\right), \\ &a_h = \frac{2\pi R}{n_h}\cos(\phi) \quad , \quad R = R_1 + x\sin(\alpha), \end{aligned} \tag{1}$$

where α is the semi vertex angle of cone, n_h is number of helical ribs, a_h spacing helical ribs, R general radius of conical shell, R_1 and R_2 are the cone radii at the small and the large cross-sections, respectively. Also, considering the geodesic path due to filament winding process assures a continuous variation of the helical angle from ϕ_1 to ϕ_2 according to Clairaut Equation and ϕ is variable helical

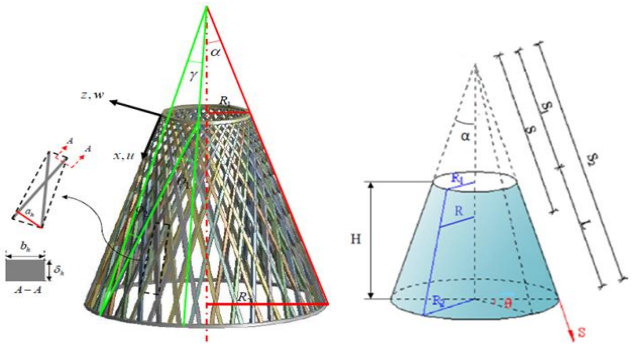

(a) (b)

Fig. 1 Geometrical characteristics of (a) composite lattice conical shell; (b) auxiliary schematic

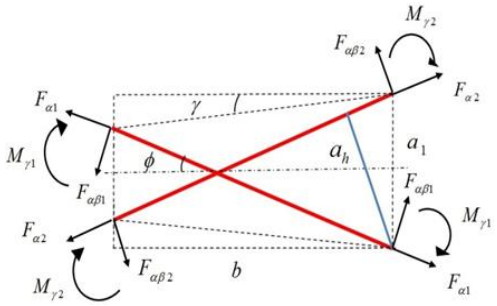

(a)

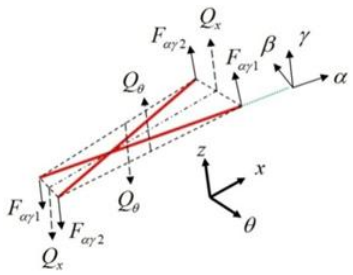

(b)

Fig. 2 Acting forces and moments on generic macro-element of conical lattice shell: (a) axial forces and in-plane bending moments; (b) shear forces on the edges

angle that is continuously changing from the top to the bottom of the structure.

3. Equivalent stiffness of composite lattice conical shell

In order to consider dynamic behavior of shell and study the vibration, at first it is required to determine the equivalent stiffness parameters of the hole structure. The analytical modeling method, i.e., the smeared stiffener approach uses a mathematical model to smear the stiffeners into an equivalent laminate and determine the equivalent stiffness of the laminate. This engages determination of stiffness contribution of the grid (stiffeners) as well as that of the shell. In developing the analytical model, a unit cell of the stiffener structure has to be defined first. The unit cell is chosen such that the whole grid structure can be reproduced by repetition of this unit cell (Figs. 1 and 2). The procedure is similar to that used in (Kidane *et al*. 2003 and Woldesenbet *et al*. 2003) but based on the following refined assumptions:

(1) The transverse modulus of the unidirectional stiffeners is much lower than the longitudinal modulus, and the cross-sectional dimensions are also very small compared to the length dimension.
(2) The stiffeners are modeled as beams and in addition to bear axial loads, considered to support shear loads and bending moments .
(3) Uniform stress is assumed across the cross-sectional area of the stiffeners.
(4) Load is transferred through shear forces between the stiffeners and the shell.
(5) The torsional stresses in the cross sections of the stiffeners are ignored.

3.1 Force analysis

The mid-plane strains and curvatures of the shell are given by ε_x^0, ε_θ^0, $\varepsilon_{x\theta}^0$, and χ_x, χ_θ, $\chi_{x\theta}$ respectively. Based on laminated plate theory, the strains on the interface of the stiffener and the shell are given by Eq. (2) (Woldesenbet *et al*. 2003).

$$\begin{aligned}&\varepsilon_x = \varepsilon_x^0 + \chi_x\left(\frac{t}{2}\right), \varepsilon_\theta = \varepsilon_\theta^0 + \chi_\theta\left(\frac{t}{2}\right),\\ &\varepsilon_{x\theta} = \varepsilon_{x\theta}^0 + \chi_{x\theta}\left(\frac{t}{2}\right), \varepsilon_{zx} = \varepsilon_{zx}^0, \varepsilon_{z\theta} = \varepsilon_{z\theta}^0,\end{aligned} \tag{2}$$

where t is the thickness of the outer laminate shell. The transformation matrix (Hemmatnezhad *et al*. 2014) is used to resolve these strains along the stiffener direction (α), and normal to the stiffener directions (β), and corresponding shear strain ($\alpha\beta$)

$$\begin{bmatrix}\varepsilon_\alpha\\ \varepsilon_\beta\\ \varepsilon_{\beta\gamma}\\ \varepsilon_{\alpha\gamma}\\ \varepsilon_{\alpha\beta}\end{bmatrix} = \begin{bmatrix}c^2 & s^2 & 0 & 0 & cs\\ s^2 & c^2 & 0 & 0 & -cs\\ 0 & 0 & c & s & 0\\ 0 & 0 & -s & c & 0\\ -2cs & -2cs & 0 & 0 & c^2-s^2\end{bmatrix}\begin{bmatrix}\varepsilon_x\\ \varepsilon_\theta\\ \varepsilon_{\theta z}\\ \varepsilon_{xz}\\ \varepsilon_{x\theta}\end{bmatrix} \tag{3}$$

where $c = \cos(\phi)$, $s = \sin(\phi)$ and ϕ is the orientation of the ribs with respect to the axial direction. Applying assumptions (2) and (3), the forces corresponding to these strains are calculated according to Eq. (4).

$$\begin{aligned}F_{\alpha 1} &= A_h E_\alpha \varepsilon_{\alpha 1} = A_h E_\alpha (c^2\varepsilon_x + s^2\varepsilon_\theta + cs\varepsilon_{x\theta}),\\ F_{\alpha 2} &= A_h E_\alpha \varepsilon_{\alpha 2} = A_h E_\alpha (c^2\varepsilon_x + s^2\varepsilon_\theta - cs\varepsilon_{x\theta}),\\ F_{\alpha\beta 1} &= A_h G_{\alpha\beta}\varepsilon_{\alpha\beta 1} = A_h G_{\alpha\beta}(-2cs\varepsilon_x - 2cs\varepsilon_\theta + (c^2-s^2)\varepsilon_{x\theta}),\\ F_{\alpha\beta 2} &= A_h G_{\alpha\beta}\varepsilon_{\alpha\beta 2} = A_h G_{\alpha\beta}(2cs\varepsilon_x + 2cs\varepsilon_\theta + (c^2-s^2)\varepsilon_{x\theta}),\end{aligned} \tag{4}$$

Where E_α and $G_{\alpha\beta}$ are the longitudinal and shear modulus of the ribs, respectively. Summing up the axial and circumferential forces on the sides of the unit cell, one can

obtain

$$F_x = (F_{\alpha 1} + F_{\alpha 2})\cos(\phi) + (F_{\alpha\beta 1} - F_{\alpha\beta 2})\sin(\phi)$$
$$F_\theta = (F_{\alpha 1} + F_{\alpha 2})\sin(\phi) + (F_{\alpha\beta 2} - F_{\alpha\beta 1})\cos(\phi) \quad (5)$$

The shear force is obtained by summing the forces along each sides of the unit cell as

$$F_{x\theta} = (F_{\alpha 2} - F_{\alpha 1})\sin(\phi) + (F_{\alpha\beta 1} + F_{\alpha\beta 2})\cos(\phi) \quad (6)$$

Using Eqs. (1)-(6) and dividing the force expressions by the corresponding edge width of the unit cell, one can write the corresponding forces per unit length as

$$\begin{aligned}
N_x^{lat} &= \frac{2}{a_h} A_h E_\alpha \cos(\phi)^4 \varepsilon_x^0 + \frac{2}{a_h} A_h E_\alpha \sin(\phi)^2 \cos(\phi)^2 \varepsilon_\theta^0 \\
&+ \frac{1}{a_h} A_h E_\alpha \cos(\phi)^4 t\chi_x + \frac{1}{a_h} A_h E_\alpha \sin(\phi)^2 \cos(\phi)^2 t\chi_\theta, \\
N_\theta^{lat} &= \frac{2}{a_h \cos(\gamma)} A_h E_\alpha \sin(\phi-\gamma)\sin(\phi)\cos(\phi)^2 \varepsilon_x^0 \\
&+ \frac{2}{a_h \cos(\gamma)} A_h E_\alpha \sin(\phi-\gamma)\sin(\phi)^3 \varepsilon_\theta^0 + \\
&\frac{1}{a_h \cos(\gamma)} A_h E_\alpha \sin(\phi-\gamma)\sin(\phi)\cos(\phi)^2 t\chi_x \\
&+ \frac{1}{a_h \cos(\gamma)} A_h E_\alpha \sin(\phi-\gamma)\sin(\phi)^3 t\chi_\theta, \\
N_{x\theta}^{lat} &= \frac{2}{a_h \cos(\gamma)} A_h E_\alpha \sin(\phi-\gamma)\sin(\phi)\cos(\phi)^2 \varepsilon_{x\theta}^0 \\
&+ \frac{1}{a_h \cos(\gamma)} A_h E_\alpha \sin(\phi-\gamma)\sin(\phi)\cos(\phi)^2 t\chi_{x\theta},
\end{aligned} \quad (7)$$

3.2 Moment analysis

The reaction moment due to the ribs is caused by the shear forces on the interface of the rib and the shell. The shear forces on the surface of the shell. Fig. 2(a), shows the different moments created by these forces. The moment caused by these forces on the mid-plane of the shell equals to the forces multiplied by one half the shell thickness. So, $M_{\gamma 1}$ and $M_{\gamma 2}$ are the moments resulting from forces $F_{\alpha 1}$ and $F_{\alpha 2}$, respectively (Kidane *et al*. 2003). Following the same procedure as the force analysis on a unit cell, the resultant moments on the horizontal and vertical sides of the unit cell are derived and depicted in Eq. (8)

$$\begin{aligned}
M_\theta^{lat} &= \frac{1}{a_h \cos(\gamma)} A_h E_\alpha \sin(\phi-\gamma)\sin(\phi)\cos(\phi)^2 t\varepsilon_x^0 \\
&+ \frac{1}{a_h \cos(\gamma)} A_h E_\alpha \sin(\phi-\gamma)\sin(\phi)^3 t\varepsilon_\theta^0 \\
&+ \frac{1}{2a_h \cos(\gamma)} A_h E_\alpha \sin(\phi-\gamma)\sin(\phi)\cos(\phi)^2 t^2 \chi_x \\
&+ \frac{1}{2a_h \cos(\gamma)} A_h E_\alpha \sin(\phi-\gamma)\sin(\phi)^3 t^2 \chi_\theta, \\
M_{x\theta}^{lat} &= \frac{1}{a_h \cos(\gamma)} A_h E_\alpha \sin(\phi-\gamma)\sin(\phi)\cos(\phi)^2 t\varepsilon_{x\theta}^0 \\
&+ \frac{1}{2a_h \cos(\gamma)} A_h E_\alpha \sin(\phi-\gamma)\sin(\phi)\cos(\phi)^2 t^2 \chi_{x\theta},
\end{aligned} \quad (8)$$

3.3 Shear force analysis

For determining shear forces on macro-element of composite lattice conical shell, the strain component $\varepsilon_{\alpha\gamma}$ can be written as (Hemmatnezhad *et al*. 2014)

$$F_{x\theta} = (F_{\alpha 2} - F_{\alpha 1})\sin(\phi) + (F_{\alpha\beta 1} + F_{\alpha\beta 2})\cos(\phi), \quad (9)$$

Considering shear strain (8), the resulting shear forces are given as)

$$\begin{aligned}
F_{\alpha\gamma 1} &= A_h G_{\alpha z}(\cos(\phi)\varepsilon_{xz} + \sin(\phi)\varepsilon_{\theta z}), \\
F_{\alpha\gamma 2} &= A_h G_{\alpha z}(\cos(\phi)\varepsilon_{xz} - \sin(\phi)\varepsilon_{\theta z}),
\end{aligned} \quad (10)$$

Considering Fig. 2(b), the shear forces in the x and θ directions and then summing up the forces on the proper latter sides of the unit cell can be written as

$$q_x^{lat} = F_{\alpha\gamma 1} + F_{\alpha\gamma 2} \quad , \quad q_\theta^{lat} = F_{\alpha\gamma 1} - F_{\alpha\gamma 2}, \quad (11)$$

Using (10) one can rewrite (11)

And the resultant shear forces per unit length can be obtained by dividing the above forces by the corresponding length as

$$q_x^{lat} = F_{\alpha\gamma 1} + F_{\alpha\gamma 2} \quad , \quad q_\theta^{lat} = F_{\alpha\gamma 1} - F_{\alpha\gamma 2}, \quad (12)$$

$$Q_x^{lat} = \frac{2A_h G_{\alpha z}\cos(\phi)}{a_1}\varepsilon_{xz}^0 \quad , \quad Q_\theta^{lat} = \frac{2A_h G_{\alpha z}\sin(\phi)}{b}\varepsilon_{\theta z}^0, \quad (13)$$

Considering geometrical characteristics of lattice part of the composite conical shell in Fig. 2(a), one can deduces

$$a_1 = \frac{a_h}{\cos(\phi)} \quad , \quad b = \frac{a_h}{\cos(\phi)(\tan(\phi) - \tan(\gamma))} \quad (14)$$

So relations (13) can be arranged in matrix form as

$$\begin{Bmatrix} Q_x^{lat} \\ Q_\theta^{lat} \end{Bmatrix} = \begin{bmatrix} \frac{2}{a_h} A_h G_{\alpha z}\cos\phi^2 & 0 \\ \frac{2}{a_h} A_h G_{\alpha z}\sin(\phi)\cos(\phi)(\tan(\phi) - \tan(\gamma)) & 0 \end{bmatrix} \begin{Bmatrix} \varepsilon_{xz}^0 \\ \varepsilon_{\theta z}^0 \end{Bmatrix} \quad (15)$$

3.4 The equivalent stiffness matrix

Eqs. (7) and (8) are, respectively, the force and moment contribution of the ribs or lattice part of conical shell, hence, denoted by the superscript "lat". Taking into account the assumptions in Section 3, these equations are rewritten in a matrix form in Eq. (16)

$$\begin{Bmatrix} N_x^{lat} \\ N_\theta^{lat} \\ N_{x\theta}^{lat} \\ M_x^{lat} \\ M_\theta^{lat} \\ M_{x\theta}^{lat} \\ Q_x^{lat} \\ Q_\theta^{lat} \end{Bmatrix} = \begin{bmatrix} a_{11} & a_{12} & 0 & a_{14} & a_{15} & 0 & 0 & 0 \\ a_{21} & a_{22} & 0 & a_{24} & a_{25} & 0 & 0 & 0 \\ 0 & 0 & a_{33} & 0 & 0 & a_{36} & 0 & 0 \\ a_{41} & a_{42} & 0 & a_{44} & a_{45} & 0 & 0 & 0 \\ a_{51} & a_{52} & 0 & a_{54} & a_{55} & 0 & 0 & 0 \\ 0 & 0 & a_{63} & 0 & 0 & a_{66} & 0 & 0 \\ 0 & 0 & 0 & 0 & 0 & 0 & a_{77} & 0 \\ 0 & 0 & 0 & 0 & 0 & 0 & 0 & a_{88} \end{bmatrix} \begin{Bmatrix} \varepsilon_{0x} \\ \varepsilon_{0\theta} \\ \gamma_{0x\theta} \\ \chi_x \\ \chi_\theta \\ \chi_{x\theta} \\ \varepsilon_{0xz} \\ \varepsilon_{0\theta z} \end{Bmatrix} \quad (16)$$

Where in (16)

$$
\begin{aligned}
&a_{11}=\frac{2}{a_h}A_hE_\alpha\cos(\phi)^4, a_{12}=\frac{2}{a_h}A_hE_\alpha\sin(\phi)^2\cos(\phi)^2,\\
&a_{14}=\frac{1}{a_h}A_hE_\alpha\cos(\phi)^4t, a_{15}=\frac{1}{a_h}A_hE_\alpha\sin(\phi)^2\cos(\phi)^2t,\\
&a_{21}=\frac{2}{a_h\cos(\gamma)}A_hE_\alpha\sin(\phi-\gamma)\sin(\phi)\cos(\phi)^2,\\
&a_{22}=\frac{2}{a_h\cos(\gamma)}A_hE_\alpha\sin(\phi-\gamma)\sin(\phi)^3,\\
&a_{24}=\frac{1}{a_h\cos(\gamma)}A_hE_\alpha\sin(\phi-\gamma)\sin(\phi)\cos(\phi)^2t, a\\
&_{25}=\frac{1}{a_h\cos(\gamma)}A_hE_\alpha\sin(\phi-\gamma)\sin(\phi)^3t,\\
&a_{33}=\frac{2}{a_h\cos(\gamma)}A_hE_\alpha\sin(\phi-\gamma)\sin(\phi)\cos(\phi)^2,\\
&a_{36}=\frac{2}{a_h\cos(\gamma)}A_hE_\alpha\sin(\phi-\gamma)\sin(\phi)\cos(\phi)^2t,\\
&a_{41}=\frac{1}{a_h}A_hE_\alpha\cos(\phi)^4t, a_{42}=\frac{1}{a_h}A_hE_\alpha\sin(\phi)^2\cos(\phi)^2t,\\
&a_{44}=\frac{1}{2a_h}A_hE_\alpha\cos(\phi)^4t^2, a_{45}=\frac{1}{2a_h}A_hE_\alpha\sin(\phi)^2\cos(\phi)^2t^2,\\
&a_{51}=\frac{1}{a_h\cos(\gamma)}A_hE_\alpha\sin(\phi-\gamma)\sin(\phi)\cos(\phi)^2t,\\
&a_{52}=\frac{1}{a_h\cos(\gamma)}A_hE_\alpha\sin(\phi-\gamma)\sin(\phi)^3t,\\
&a_{54}=\frac{1}{2a_h\cos(\gamma)}A_hE_\alpha\sin(\phi-\gamma)\sin(\phi)\cos(\phi)^2t^2,\\
&a_{55}=\frac{1}{2a_h\cos(\gamma)}A_hE_\alpha\sin(\phi-\gamma)\sin(\phi)^3t^2,\\
&a_{63}=\frac{1}{a_h\cos(\gamma)}A_hE_\alpha\sin(\phi-\gamma)\sin(\phi)\cos(\phi)^2t,\\
&a_{66}=\frac{1}{2a_h\cos(\gamma)}A_hE_\alpha\sin(\phi-\gamma)\sin(\phi)\cos(\phi)^2t^2,\\
&a_{77}=\frac{2}{a_h}A_hG_{\alpha z}\cos\phi^2, a_{88}=\frac{2}{a_h}A_hG_{\alpha z}\sin\phi\cos\phi(\tan\phi-\tan\gamma),\\
&A_h=b_h\cdot\delta_h,
\end{aligned}
\tag{17}
$$

It is clear that despite of cylindrical shells, the coefficients of stiffness of lattice composite conical shell i.e. the equivalent Stiffness matrix of conical shells is not constant and changes along the length of the cone. For checking the accuracy of coefficients of stiffness in (16) and (17), one can suppose $\gamma=0$, i.e., cylindrical shell and the coefficients of stiffness for cylindrical composite lattice shell could be obtained (Kidan *et al*. 2003). Also, the resultant force and moments due to the outer shell in terms of the strain components of the mid-plane surface of the shell are obtained. For orthotropic symmetrical laminated outer skin, the physical relations i.e., hook law, have following forms

$$
\begin{Bmatrix} N_x^{sh}\\ N_\theta^{sh}\\ N_{x\theta}^{sh}\\ M_x^{sh}\\ M_\theta^{sh}\\ M_{x\theta}^{sh}\\ Q_x^{sh}\\ Q_\theta^{sh}\end{Bmatrix}=
\begin{bmatrix}
b_{11} & b_{12} & 0 & c_{11} & c_{12} & 0 & 0 & 0\\
b_{21} & b_{22} & 0 & c_{21} & c_{22} & 0 & 0 & 0\\
0 & 0 & b_{33} & 0 & 0 & c_{33} & 0 & 0\\
c_{11} & c_{12} & 0 & d_{11} & d_{12} & 0 & 0 & 0\\
c_{21} & c_{22} & 0 & d_{21} & d_{22} & 0 & 0 & 0\\
0 & 0 & c_{33} & 0 & 0 & d_{33} & 0 & 0\\
0 & 0 & 0 & 0 & 0 & 0 & b'_{77} & 0\\
0 & 0 & 0 & 0 & 0 & 0 & 0 & b'_{88}
\end{bmatrix}
\begin{Bmatrix} \varepsilon_{0x}\\ \varepsilon_{0\theta}\\ \gamma_{0x\theta}\\ \chi_x\\ \chi_\theta\\ \chi_{x\theta}\\ \varepsilon_{0xz}\\ \varepsilon_{0\theta z}\end{Bmatrix}
\tag{18}
$$

in which $b'_{77}=Kb_{77}, b'_{88}=Kb_{88}$ and K is known as a shear correction factor (Qatu 2004). In relations (16), (18) the superscripts 'lat' stands for the ribs and 'sh' for outer skin. Moreover, the mentioned coefficients of stiffness of the shell are given as

$$
(b_{ij}, c_{ij}, d_{ij})=\int_{-\frac{t}{2}}^{\frac{t}{2}} Q_{ij}(1, z, z^2)dz \tag{19}
$$

where Q_{ij} are the plane stress-reduced stiffness, and t is the uniform thickness of the shell with the reference middle surface. The total force and moment on the panel is the superposition of the force and moment due to the ribs and the shell as shown by Eq. (20)

$$
\begin{bmatrix} N\\ M\end{bmatrix}=\begin{bmatrix} N^{lat}+N^{sh}\\ M^{lat}+M^{sh}\end{bmatrix}\ ,\ \begin{bmatrix} Q_x\\ Q_\theta\end{bmatrix}=\begin{bmatrix} Q_x^{lat}+Q_x^{sh}\\ Q_\theta^{lat}+Q_\theta^{sh}\end{bmatrix} \tag{20}
$$

So the resultant stiffness parameters obtained from above equations are the equivalent stiffness parameters of the whole conical shell and constitutive equations have the following general form

$$
\begin{bmatrix} N\\ M\\ Q\end{bmatrix}=\begin{bmatrix} B & C & 0\\ C & D & 0\\ 0 & 0 & A\end{bmatrix}\begin{bmatrix} \varepsilon\\ \chi\\ \gamma\end{bmatrix} \tag{21}
$$

Here N and ε are membrane stress resultants and strains of the reference surface, M and χ are moments and the corresponding bending deformations, Q and γ are transverse forces and shear strains. B- membrane, C- coupling and D- bending stiffness coefficients. These coefficients could be defined as following relations.

$$
\begin{aligned}
&B_{11}=a_{11}+b_{11}, C_{11}=a_{14}+c_{11}, D_{11}=a_{44}+d_{11},\\
&B_{12}=a_{12}+b_{12}, C_{12}=a_{15}+c_{12}, D_{12}=a_{45}+d_{12},\\
&B_{21}=a_{21}+b_{21}, C_{21}=a_{24}+c_{21}, D_{21}=a_{54}+d_{21},\\
&B_{22}=a_{22}+b_{22}, C_{22}=a_{25}+c_{22}, D_{22}=a_{55}+d_{22},\\
&B_{33}=a_{33}+b_{33}, C_{33}=a_{36}+c_{33}, D_{33}=a_{66}+d_{33},
\end{aligned}
\tag{21}
$$

4. Basic equations of thick (shear deformation) conical shell

4.1 Equations of motion

A lattice composite conical shell is depicted in Fig. 3. The conical shell is referred to a coordinate system (s, θ, z). Also for more explanation the auxiliary schematic, (Fig. 1(b)) is considered here. The equilibrium equations of motion for thick conical shells in terms of the resultant forces and moments including the transverse shear and rotary inertia terms are (Qatu 2004)

$$\begin{aligned}
&\frac{\partial N_s}{\partial s}+\frac{1}{s\sin(\alpha)}\frac{\partial N_{s\theta}}{\partial \theta}+\frac{N_s-N_\theta}{s}+q_s=I_1\ddot{u}^2+I_2\ddot{\psi}_s^2,\\
&\frac{1}{s\sin(\alpha)}\frac{\partial N_\theta}{\partial \theta}+\frac{\partial N_{s\theta}}{\partial s}+\frac{N_{s\theta}+N_{\theta s}}{s}+\frac{Q_\theta}{s\tan(\alpha)}\\
&+q_\theta=I_1\ddot{v}^2+I_2\ddot{\psi}_\theta^2,\\
&\frac{\partial M_s}{\partial s}+\frac{1}{s\sin(\alpha)}\frac{\partial M_{s\theta}}{\partial \theta}+\frac{M_s-M_\theta}{s}-Q_s\\
&+m_s=I_2\ddot{u}^2+I_3\ddot{\psi}_s^2,\\
&\frac{1}{s\sin(\alpha)}\frac{\partial M_\theta}{\partial \theta}+\frac{\partial M_{s\theta}}{\partial s}+\frac{M_{s\theta}+M_{\theta s}}{s}-Q_\theta\\
&+m_\theta=I_2\ddot{v}^2+I_3\ddot{\psi}_\theta^2,\\
&\frac{\partial Q_s}{\partial s}+\frac{1}{s\sin(\alpha)}\frac{\partial Q_\theta}{\partial \theta}-\frac{N_\theta}{s\tan(\alpha)}+\frac{Q_s}{s}=I_1\ddot{w}^2
\end{aligned} \tag{23}$$

Where in (23) N_s, N_θ, M_s, M_θ represent the resultant forces and moments, $N_{s\theta}$ and $N_{\theta s}$ resultant membrane forces, Q_s and Q_θ the resultant transverse shearing forces, m_S and m_θ represent possible body couples (moments per unit length), q_s and q_θ are the distributed forces in the s and θ directions, respectively. For deriving the equations of motion of composite conical lattice shell, it is assumed that vibration of the shell is accompanied by a large number of relatively small waves, that such wave lengths which at least in one direction is small compared with the radius of curvature of the middle surface or dimensions of the shell. So, one can suppose that each small semi-waves of shell can be considered as a shallow shell, that permits to apply to it the basic principles of the theory of shallow shells. Finally, the equations of motion of shear deformable conical lattice shells can be rewritten as follow

$$\begin{aligned}
&\frac{\partial N_S}{\partial S}+\frac{1}{S\sin(\alpha)}\frac{\partial N_{S\theta}}{\partial \theta}=I_1\ddot{u}^2+I_2\ddot{\psi}_s^2,\\
&\frac{1}{S\sin(\alpha)}\frac{\partial}{\partial \theta}(N_\theta)+\frac{\partial N_{S\theta}}{\partial S}=I_1\ddot{v}^2+I_2\ddot{\psi}_\theta^2,\\
&\frac{\partial M_S}{\partial s}+\frac{1}{S\sin(\alpha)}\frac{\partial M_{S\theta}}{\partial \theta}-Q_S=I_2\ddot{u}^2+I_3\ddot{\psi}_s^2,\\
&\frac{1}{S\sin(\alpha)}\frac{\partial M_\theta}{\partial \theta}+\frac{\partial M_{S\theta}}{\partial s}-Q_\theta=I_2\ddot{v}^2+I_3\ddot{\psi}_\theta^2,\\
&\frac{\partial Q_S}{\partial S}+\frac{1}{S\sin(\alpha)}\frac{\partial Q_\theta}{\partial \theta}+\frac{N_\theta}{S\tan(\alpha)}=I_1\ddot{w}^2
\end{aligned} \tag{24}$$

where I_1, I_2, I_3 are the inertia terms obtained as

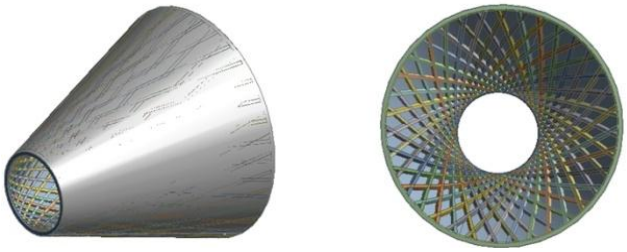

Fig. 3 A 3D-model of the composite lattice conical shell with outer laminated skin

$$(I_1,I_2,I_3)=\int_{-\frac{t}{2}}^{\frac{t}{2}}\rho(z)(1,z,z^2)dz \tag{25}$$

4.2 Kinematic relations

The components of the deformation of the conical shell with references to this given coordinate system are denoted by u, v, w in the s, θ and z directions, respectively. Based on the first-order shear deformation theory and Applying the shallow shell assumption in Section 4.1, the strains and curvatures on the mid-plane surface of the thick conical shell can be written as (Qatu 2004)

$$\begin{aligned}
&\varepsilon_s^0=\frac{\partial u_0}{\partial s},\\
&\varepsilon_\theta^0=\frac{1}{s\sin(\alpha)}\frac{\partial v_0}{\partial \theta}+\frac{w_0}{s\tan(\alpha)},\\
&\varepsilon_{s\theta}^0=\frac{\partial v_0}{\partial s}+\frac{1}{s\sin(\alpha)}\frac{\partial u_0}{\partial \theta},\\
&\varepsilon_{sz}^0=\frac{\partial w_0}{\partial s}+\psi_s,\\
&\varepsilon_{\theta z}^0=\frac{1}{s\sin(\alpha)}\frac{\partial w_0}{\partial \theta}+\psi_\theta,\\
&\chi_s=\frac{\partial \psi_s}{\partial s},\\
&\chi_\theta=\frac{1}{s\sin(\alpha)}\frac{\partial \psi_\theta}{\partial \theta}+\frac{\psi_s}{s},\\
&\chi_{s\theta}=\frac{\partial \psi_\theta}{\partial s}+\frac{1}{s\sin(\alpha)}\frac{\partial \psi_S}{\partial \theta}-\frac{\psi_\theta}{s},
\end{aligned} \tag{26}$$

It is assumed that there are no stretching-shearing, twisting-shearing, bending-shearing, and bending-twisting couplings, so stress resultant-strain relations (the constitutive relations) may be represented as (Tong 1994)

$$\begin{Bmatrix} N_s\\ N_\theta\\ N_{s\theta}\\ M_s\\ M_\theta\\ M_{s\theta}\\ Q_s\\ Q_\theta \end{Bmatrix}=\begin{bmatrix} B_{11} & B_{12} & 0 & C_{11} & C_{12} & 0 & 0 & 0\\ B_{12} & B_{22} & 0 & C_{12} & C_{22} & 0 & 0 & 0\\ 0 & 0 & B_{33} & 0 & 0 & C_{33} & 0 & 0\\ C_{11} & C_{12} & 0 & D_{11} & D_{12} & 0 & 0 & 0\\ C_{12} & C_{22} & 0 & D_{12} & D_{22} & 0 & 0 & 0\\ 0 & 0 & C_{33} & 0 & 0 & D_{33} & 0 & 0\\ 0 & 0 & 0 & 0 & 0 & 0 & B_{77} & 0\\ 0 & 0 & 0 & 0 & 0 & 0 & 0 & B_{88} \end{bmatrix}\begin{Bmatrix} \varepsilon_s^0\\ \varepsilon_\theta^0\\ \varepsilon_{s\theta}^0\\ \chi_s\\ \chi_\theta\\ \chi_{s\theta}\\ \varepsilon_{sz}^0\\ \varepsilon_{\theta z}^0 \end{Bmatrix} \tag{27}$$

In conical shell, for convenience the independent variable is assumed as $S = S_1 e^x$. When changing S from S_1 to S_2, the coordinate x within the length of the truncated cone varies from zero to $x_0 = ln\, S_2/S_1$. Using Eq. (26) and taking into account the variable x instead of S, equation of motions (24) can be expressed in terms of displacement fields $u,\ v,\ w,\ \psi_x,\ \psi_\theta$ and its derivations as follows

$$
\begin{aligned}
&B_{11}(u_{,xx}-u_{,x})+B_{12}(-\frac{1}{\sin(\alpha)}v_{,\theta}+\frac{1}{\sin(\alpha)}v_{,x\theta}+\\
&\frac{1}{\tan(\alpha)}w_{,x}-\frac{1}{\sin(\alpha)}w)+C_{11}(\psi_{x,xx}-\psi_{x,x})+\\
&C_{12}(-\frac{1}{\sin(\alpha)}\psi_{\theta,\theta}+\frac{1}{\sin(\alpha)}\psi_{\theta,\theta x}+\psi_{x,x}-\psi_x)+\\
&\frac{1}{\sin(\alpha)}B_{33}(v_{,\theta x}+\frac{1}{\sin(\alpha)}u_{,\theta\theta})+\frac{1}{\sin(\alpha)}\\
&C_{33}(\psi_{\theta,\theta x}+\frac{1}{\sin(\alpha)}\psi_{x,\theta\theta}-\psi_{\theta,\theta})=S_1^2e^{2x}(I_1u_{,tt}-I_2\psi_{x,tt}),\\
&\frac{1}{\sin(\alpha)}B_{21}u_{,\theta x}+B_{22}(\frac{1}{\sin(\alpha)}v_{,\theta\theta}+\frac{1}{\tan(\alpha)}w_{,\theta})+\\
&B_{33}(v_{,xx}-v_{,x}-\frac{1}{\sin(\alpha)}u_{,\theta}+\frac{1}{\sin(\alpha)}u_{,x\theta})+C_{21}\psi_{x,\theta x}+\\
&C_{22}(\frac{1}{\sin(\alpha)}\psi_{\theta,\theta\theta}+\psi_{x,\theta})+C_{33}(\psi_{\theta,xx}-2\psi_{\theta,x}\\
&-\frac{1}{\sin(\alpha)}\psi_{x,x\theta}+\psi_\theta)=S_1^2e^{2x}(I_1v_{,tt}+I_2\psi_{\theta,tt}),C_{11}(u_{,xx}-u_{,x})+\\
&C_{12}(-\frac{1}{\sin(\alpha)}v_{,\theta}+\frac{1}{\sin(\alpha)}v_{,\theta x}+\frac{w_{,x}}{\tan(\alpha)}-\frac{w}{\tan(\alpha)})+\\
&D_{11}(\psi_{x,xx}-\psi_{x,x})+D_{12}(-\frac{1}{\sin(\alpha)}\psi_{\theta,\theta}+\frac{1}{\sin(\alpha)}\psi_{\theta,\theta x}\\
&+\psi_{x,x}-\psi_x)+\frac{1}{\sin(\alpha)}C_{33}(v_{,\theta x}+\frac{1}{\sin(\alpha)}u_{,\theta\theta})+\\
&\frac{1}{\sin(\alpha)}D_{33}(\psi_{\theta,\theta x}+\frac{1}{\sin(\alpha)}\psi_{x,\theta\theta}-\psi_{\theta,\theta})-\\
&B_{77}(w_{,x}+S_1e^x\psi_x)=S_1^2e^{2x}(I_2u_{,tt}+I_3\psi_{x,tt}),\\
&\frac{1}{\sin(\alpha)}C_{12}(u_{,x\theta}-u_{,x})+C_{22}(\frac{1}{\sin(\alpha)}v_{,\theta\theta}+\frac{1}{\tan(\alpha)}w_{,\theta})+\\
&\frac{1}{\sin(\alpha)}D_{12}\psi_{x,x\theta}+\frac{1}{\sin(\alpha)}D_{22}(\frac{1}{\sin(\alpha)}\psi_{\theta,\theta\theta}+\psi_{x,\theta})+\\
&\frac{1}{\sin(\alpha)}C_{33}(v_{,xx}-\frac{1}{\sin(\alpha)}v_{,x}-\frac{1}{\sin(\alpha)}u_{,\theta}+\\
&\frac{1}{\sin(\alpha)}\psi_x)+\frac{1}{\sin(\alpha)}D_{33}(\psi_{\theta,xx}-2\psi_{\theta,x}-\frac{1}{\sin(\alpha)}\psi_{x,\theta}+\\
&\frac{1}{\sin(\alpha)}\psi_{\theta,x\theta}+\psi_\theta)=S_1^2e^{2x}(I_2v_{,tt}+I_3\psi_{\theta,tt}),\\
&\frac{1}{\sin(\alpha)}(B_{12}u_{,x}+B_{22}(\frac{1}{\sin(\alpha)}v_{,\theta}+\frac{1}{tan(\alpha)}w)+C_{12}\psi_{x,x}+\\
&C_{22}(\frac{1}{\sin(\alpha)}\psi_{\theta,\theta}+\frac{1}{tan(\alpha)}\psi_x))+B_{77}(w_{,xx}-w_{,x}+\psi_{x,x})+\\
&\frac{1}{\sin(\alpha)}B_{88}(\frac{1}{\sin(\alpha)}w_{,\theta\theta}+\psi_{\theta,\theta})=S_1^2e^{2x}I_1w_{,tt},
\end{aligned}
\tag{28}
$$

4.2 Analytical approach

Defining displacements fields for circular composite lattice conical shell for any circumferential and axial wave numbers n and m respectively as

$$
\begin{aligned}
u(x,\theta,t)&=\Re_u(x)\cos(\eta\theta)\cos(\omega t),\\
v(x,\theta,t)&=\Re_v(x)\sin(\eta\theta)\cos(\omega t),\\
w(x,\theta,t)&=\Re_w(x)\cos(\eta\theta)\cos(\omega t),\\
\psi_x(x,\theta,t)&=\Re_{\psi_x}(x)\cos(\eta\theta)\cos(\omega t),\\
\psi_\theta(x,\theta,t)&=\Re_{\psi_\theta}(x)\cos(\eta\theta)\cos(\omega t),
\end{aligned}
\tag{29}
$$

where $\Re_u(x), \Re_v(x), \Re_w(x), \Re_{\psi_x}(x)$ and $\Re_{\psi_\theta}(x)$ are the axial modal functions and ω is the natural frequency. The most important and difficult part of this analysis engages to choosing desirable series forms for modal functions. An appropriate set of Fourier series which satisfies the boundary conditions of a shell with simply-supported ends with no axial constraint (SNA-SNA) term-by-term can be given as (Hemmatnezhad *et al*. 2014)

$$
\begin{aligned}
\Re_u(x)&=U_{0n}+\sum_{m=1}^{\infty}\sum_{n=1}^{\infty}U_{mn}\cos(\lambda x),\\
\Re_v(x)&=\sum_{m=1}^{\infty}\sum_{n=1}^{\infty}V_{mn}\sin(\lambda x),\\
\Re_w(x)&=\sum_{m=1}^{\infty}\sum_{n=1}^{\infty}W_{mn}\sin(\lambda x),\\
\Re_{\psi_x}(x)&=\Psi^1_{0n}+\sum_{m=1}^{\infty}\sum_{n=1}^{\infty}\Psi^1_{mn}\cos(\lambda x),\\
\Re_{\psi_\theta}(x)&=\sum_{m=1}^{\infty}\sum_{n=1}^{\infty}\Psi^2_{mn}\sin(\lambda x),
\end{aligned}
\tag{30}
$$

where in (29) and (30)

$$
\lambda=\frac{m\pi}{x_0}\quad,\quad \eta=n,
\tag{31}
$$

Substituting displacement functions (29) and their derivatives into Eqs. (28) and after appropriate mathematical calculation, the natural frequencies of SNA–SNA composite lattice conical shell would be derived. It is implicit that, these boundary conditions do not have generality, especially when the goal is to consider general cases of boundary conditions instead of particular ones. On the other hand, sine series have zero values at the end borders unless when necessary to specify affected boundary conditions as

$$
\begin{aligned}
&\Re_v(0)=v^0,\Re_v(x_0)=v^{x_0},\\
&\Re_w(0)=w^0,\Re_w(x_0)=w^{x_0},\\
&\Re_{\psi_\theta}(0)=\psi_\theta^0,\Re_{\psi_\theta}(x_0)=\psi_\theta^{x_0},
\end{aligned}
\tag{32}
$$

For investigation of the general cases, it is necessary to maximize the generality of the formulation. For this, a shell with freely supported ends with no tangential constraint (FSNT) is chosen (Hemmatnezhad *et al*. 2014). The boundary conditions for such a shell is given by

$$u = \psi_x = Q_x = N_{x\theta} = M_{x\theta} = 0, \qquad (x = 0, x_0) \tag{33}$$

Each of the ten boundary conditions given in (33), on a term- by-term basis are satisfied by (32), so the Stokes' transformation is used to apply constrains to satisfy the boundary conditions. To differentiate the displacement functions, the border values (32) are required (the results depicted in Appendix A). The substitution of the set of displacement functions and their derivatives into Eqs. (28), gives two separated matrix equation, in which the coefficients of Fourier series are coupled as

$$\begin{pmatrix} K_{11} & K_{12} & K_{13} & K_{14} & K_{15} \\ K_{21} & K_{22} & K_{23} & K_{24} & K_{25} \\ K_{31} & K_{32} & K_{33} & K_{34} & K_{35} \\ K_{41} & K_{34} & K_{43} & K_{44} & K_{45} \\ K_{51} & K_{35} & K_{53} & K_{54} & K_{55} \end{pmatrix} \begin{bmatrix} U_{mn} \\ V_{mn} \\ W_{mn} \\ \Psi^1_{mn} \\ \Psi^2_{mn} \end{bmatrix} = \begin{bmatrix} C_1 \\ C_2 \\ C_3 \\ C_4 \\ C_5 \end{bmatrix} \tag{34}$$

and

$$\begin{pmatrix} K_{01} & K_{02} \\ K_{02} & K_{03} \end{pmatrix} \begin{bmatrix} U_{0n} \\ \Psi^1_{0n} \end{bmatrix} = \begin{bmatrix} C_6 \\ C_7 \end{bmatrix} \tag{35}$$

where in (28) and (29) due to applying the Stokes' transformation the values of C_i $(i = 1, \ldots, 7)$ are in terms of unspecified border values, N_x^0, N_x^{x0}, M_x^0, M_x^{x0}, v^0, v^{x0}, w^0, w^{x0}, ψ_θ^0, ψ_θ^{x0} and coefficients K_{ij} $(i, j = 1, \ldots, 5)$, K_{01}, K_{02} and K_{03} depend upon the shell frequency, geometrical and physical parameters of composite lattice conical shell and wave numbers in the circumferential and axial directions. Obviously from Eqs. (30) and (31), Fourier coefficients U_{mn}, U_{0n}, V_{mn}, W_{mn}, Ψ^1_{mn}, Ψ^2_{mn} and Ψ^1_{0n} can be expressed explicitly in terms of the ten unspecified geometric and natural boundary values N_x^0, N_x^{x0}, M_x^0, M_x^{x0}, v^0, v^{x0}, w^0, w^{x0}, ψ_θ^{x0}. Only, it is needed to apply the geometrical and natural boundary conditions in accordance with the selected general model. For further details, the reader is referred to Refs. (Ansari and Darvizeh 2008, Kadoli and Ganesan 2003). As mentioned before, choosing at both ends the natural boundary conditions as $Q_x = N_{x\theta} = M_{x\theta}$ and the geometrical ones as $u = \Psi_x = 0$, a general eigenvalue problem which can be used for any possible combination of boundary conditions, would be driven. After applying the constraints due to the geometrical and natural boundary conditions, one obtains the following homogeneous matrix equation

$$\left[\lambda_{ij}\right]\left[N_x^0 \quad N_x^{x_0} \quad M_x^0 \quad M_x^{x_0} \quad v^0 \quad v^{x_0} \quad w^0 \quad w^{x_0} \quad \psi_\theta^0 \quad \psi_\theta^{x_0}\right]^T = [0] \tag{36}$$

It is explicit that for non-trivial solution of (36), the determinant of the coefficients matrix must be equal to zero

$$\left|\lambda_{ij}\right| = 0 \qquad , \qquad (i, j = 1, \ldots, 10), \tag{37}$$

Solving (37), a characteristic equation whose eigen-values are the natural frequencies of the shell with freely supported ends with no tangential constraint will be driven. The corresponding eigenvectors, also, determine the mode shapes. It is clearly that the characteristic Eq. (37) required for any type of boundary conditions. To drive the appropriate characteristic equation for a specified boundary condition, its associated border conditions must be imposed. This can be performed (Kadoli and Ganesan 2003) by appropriately tailoring the general determinant of (37).

5. Numerical results and discussion

5.1 Calculation of the natural frequencies

In this section some results and considerations for free vibrations of composite conical lattice shell are presented. In this section and in the successive sections and examples it is considered that $m = 1$. The vibration characteristics have been performed for the filament wound composite lattice conical shell, whose schematic shown in Fig. 3. The dimensions of the shell under consideration are: $L = 1.616$ m, $R_1 = 0.3$ m, $R_2 = 0.8$ m and $\alpha = 18^\circ$. The shell is made of unidirectional carbon-fiber reinforced plastic (CFRP) having the following properties: modulus of elasticity, $E_\alpha = 100$ GPa, shear moduli $G_{\alpha\beta} = G_{\alpha\gamma} = 5.5$ MPa, $G_{\beta\gamma} = 2.5$ GPa, Poisson's ratio $\mu_{\alpha\beta} = 0.1$, $\mu_{\alpha\gamma} = 0.3$, $\mu_{\beta\gamma} = 0.3$, and density $\rho = 1450$ kg/m^3. The number of helical ribs of one helical direction (either $+\phi$, or $-\phi$) is $n_h = 35$. This is expected since the increase in helical angle for the shell composed of one and the same number of helical ribs leads to the increase in the number of their intersections. The outer laminated skin of conical shell is assumed to be layup with 90° with respect to *x*-direction with various thicknesses, while in the lattice structure, fibers are considered to be oriented in the ribs' directions. As mentioned before, in the conical shells despite of cylindrical ones, the helical angle is not constant and continuously changes, so as a consequence, the equations for the structural stiffness are more complicated than those for the cylindrical structure. In this section and successive sections, it is assumed that $m = 1$, so only the effect of the circumferential wave numbers on the natural frequencies would be considered. In Table 1 is depicted the natural frequencies calculated via the present analytical approach for various circumferential wave numbers for a SNA–SNA boundary condition. Because of the geodesic angle of helical ribs (ϕ) is not constant and is changing along the generator of cone, for calculating the variable coefficients of stiffness of the conical lattice shell, conditionally the dimensionless length of lattice cone in eleven points is divided into 10 parts from 0 to 1 with a increment equal 0.1. Composite lattice conical shell is considered with and without outer laminated skin. Note that in Table 1, in comparison between conical shells with and without outer skin, the heights of helical ribs and obviously A_h have different values. This is because of that the mass of two shells will be the same. The average values of the natural frequencies in Table 1 show that the application of the smear method for determining of the coefficients of stiffness of the conical shell without outer skin is not recommend. For more explanation, Fig. 4 shows the

Table 1 The natural frequencies via the present analytical approach for various circumferential wave numbers along the dimensionless length of composite lattice conical shell for a SNA–SNA boundary condition ($\alpha = 18^{\circ}$, $L\sin(\alpha)/R_2$ = 0.625, for without skin shell: $A_h = 20 \times 20$ mm^2 and for shell with skin: $A_h = 20 \times 12.7$ mm^2, t = 1 mm)

x^*	$n = 1$		$n = 2$		$n = 3$		$n = 4$	
	Skinless	Skin	Skinless	Skin	Skinless	Skin	Skinless	Skin
0	220.4014	209.5682	333.4727	249.5012	407.0905	353.4374	434.9248	408.9841
0.1	189.3275	190.9113	333.0988	249.1933	393.7298	352.1169	431.8315	406.9554
0.2	149.5023	172.4961	291.6497	248.7166	383.9115	351.8745	402.0674	404.8880
0.3	104.5085	156.6589	214.5620	248.6841	318.7630	347.8115	394.3706	400.9109
0.4	85.9347	144.2149	91.6489	248.2423	134.6493	347.3245	177.9584	392.1831
0.5	85.1917	135.2761	42.0534	247.6428	32.6335	341.6053	29.1472	390.2960
0.6	85.0328	129.5188	41.9969	246.7222	32.3419	337.9379	28.8336	379.3851
0.7	81.6379	126.3281	41.2008	245.3091	32.1524	333.6525	28.7317	368.1107
0.8	74.2449	125.1446	40.5336	244.0780	30.8771	321.7387	27.2238	366.4352
0.9	59.6128	124.9686	36.7943	243.2857	27.5531	294.4287	24.0098	328.7728
1	49.9410	124.7538	28.8833	229.6156	20.8616	247.8133	17.7491	260.2861
A.fr	**107.753**	**149.7601**	**108.7177**	**245.5446**	**164.9605**	**325.8354**	**181.5357**	**343.4940**

* **A.fr**: Average frequency

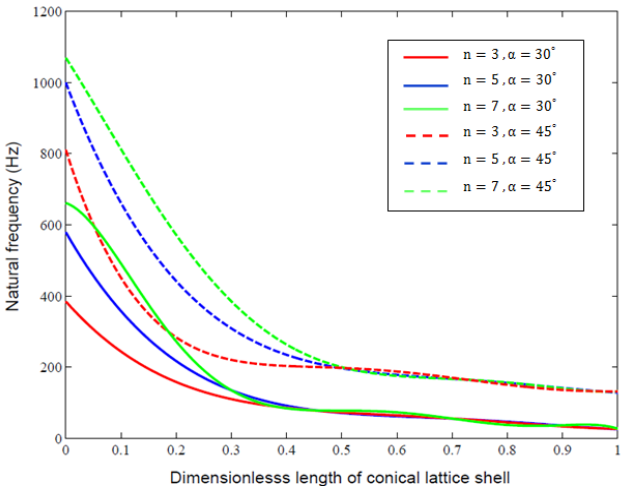

Fig. 6 Effect of semi vertex angle on the natural frequency of SNA–SNA skinless composite lattice conical shell respect to dimensionless length ($\alpha = 30^{\circ}$, 45°, $L\sin(\alpha)/R_2$ = 0.625, $A_h = 20 \times 20$ mm^2, $t = 0$ mm)

variation of the natural frequencies respect to dimensionless length of conical shell for circumferential wave numbers from 5 to 7. From the results of Table 1 and Fig. 4, it is clear that the natural frequencies of composite lattice conical shell without outer laminated skin converge for all circumferential wave numbers greater than 5 and no sensitive to variation of circumferential wave numbers. On the other hand, the difference between the calculated natural frequencies of the conical lattice shell without outer laminated skin in comparison with those of conical shell with outer skin is significant. This behavior mainly is dependent on the applying the smear method for determining the coefficients of stiffness of lattice shell. While the conical composite lattice shell have not external skin, i.e., $t = 0$, all coefficients of stiffness associated with the moments in relations (16) are zero and this causes the error in the calculations. Furthermore, in Fig. 5 is depicted the comparison of the natural frequencies versus circumferential wave numbers obtained via the present analytical approach and FEM software for a SNA–SNA conical composite lattice shell. The conical lattice structure is considered with and without outer laminated skin. Again, the difference between results, shows that the smear method is not suitable for determining the coefficients of stiffness of lattice shells without outer skin and leads to errors in determination of the natural frequencies. Fig. 6 illustrates the effect of semi vertex angle on the natural frequencies of the composite lattice conical shell. There is a comparison of the natural frequencies via the present analytical approach for various circumferential wave numbers with respect to the dimensionless length of composite lattice conical shell without outer skin for a SNA – SNA boundary condition and two different semi vertex angle of cone.

It is obvious, that the semi vertex angle of cone has significant effect on the natural frequencies of the conical shell. When the mass of the conical shell does not change, increasing the semi vertex angle of cone, leads to an increase of the natural frequencies. This is mainly because of the fact that although R_2 and the geometrical ratio $L\sin(\alpha)/R_2$ for both shells does not change, increasing the semi vertex angle of shell leads to decreasing the length of conical lattice shell. The shorter length causes closer and more compact cells of the lattice structure and finally, while the mass of shells changes insignificantly, stiffness of lattice shell with the bigger semi vertex angle would be increased. Furthermore decreasing of the length of shell, increases the influence of edge effects. For, more interpretation, Fig. 7 depicts the natural frequencies with respect to dimensionless length of composite lattice conical shell for various

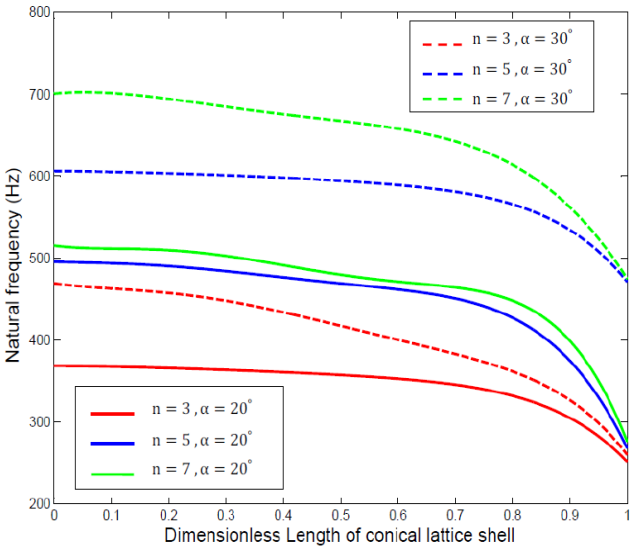

Fig. 7 Effect of semi vertex angle on the natural frequency of SNA–SNA composite lattice conical shell respect to dimensionless length of shell with outer skin ($t = 1$ mm, $L\sin(\alpha)/R_2 = 0.625$, for $\alpha = 20^\circ$: $A_h = 20 \times 14$ mm^2 and for $\alpha = 30^\circ$: $A_h = 20 \times 15.5$ mm^2)

semi vertex angles and circumferential wave numbers.

Furthermore, Fig. 8 exhibits the variation of the natural frequencies respect to the thickness of outer skin of a SNA–SNA composite conical lattice shell. The semi vertex angles equal to 18° and 30°. It could be seen, when the mass of lattice conical shell does not change, the increment of the semi vertex angle and thickness of the outer skin leads to increase of the natural frequencies.

5.2 Validations

To demonstrate the performance of the present study the numerical results are compared with the results of Hemmatnezhad *et al*. (2014) and a 3-D finite element models made by FEM software.

5.2.1 Results for lattice composite cylindrical shells

In order to check on the numerical accuracy of the present analysis, Table 4 is listed. The obtained results of the natural frequencies of composite lattice cylindrical shell via the present method are compared with those given by Hemmatnezhad *et al*. (2014).

The results are performed for four different circumferential wave numbers and three thicknesses of outer skin. This table shows the comparison of the natural frequencies of SNA-SNA lattice composite cylindrical shell. The

Table 2 Material properties of Hs-Graphite/epoxy

Young's modulus (GPa)	E_{11}, E_{22}, E_{33}	181.0, 10.34, 10.34
Shear modulus (Gpa)	G_{12}, G_{13}, G_{23}	7.7, 7.2, 7.2
Poisson's ratio	μ_{12}, μ_{13}, μ_{23}	0.28, 0.28, 0.28
Density (kg/m^3)	ρ	1389.23

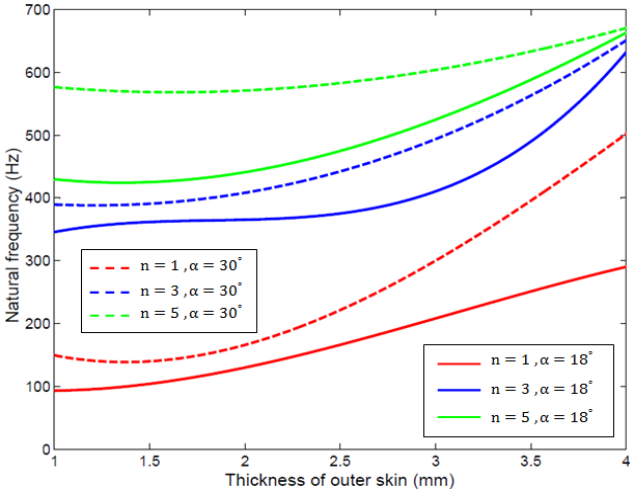

Fig. 8 Variation of the natural frequency respect to the thickness of outer skin for a SNA–SNA conical lattice shell ($L\sin(\alpha)/R_2 = 0.625$, for $\alpha = 18^\circ$: $t = 1$, $A_h = 20 \times 12.7$ mm^2, $t = 2$, $A_h = 20 \times 6.5$ mm^2, $t = 3$, $A_h = 20 \times 2.7$ mm^2, $t = 4$, $A_h = 20 \times 0.5$ mm^2, for $\alpha = 30^\circ$: $t = 1$, $A_h = 20 \times 15.5$ mm^2 and $t = 2$, $A_h = 20 \times 11.8$ mm^2, $t = 3$, $A_h = 20 \times 8$ mm^2, $t = 4$, $A_h = 20 \times 4$ mm^2)

cylindrical composite lattice shell is considered to be made of Hs-Graphite/epoxy with material properties listed in Table 2. The cylindrical shell is assumed to be four-layered with $[30/-30]_S$ stacking sequence, while in the lattice structure, fibers are considered to be oriented in the rib's' directions. The geometrical parameters associated with the cylindrical model are taken as those reported in Table 3.

5.2.2 Results for lattice composite conical shells

Since there are no enough results in open literature to illustrate the accuracy and application of present method, a finite element model is employed to build a 3-D finite element model of conical shell and as earlier mentioned is depicted in Fig. 3. The finite element analysis (FEA) is performed using ANSYS 14.0 software. The finite element model consisting of eight nodes elements (Hex8) with six degrees of freedom at each node and is meshed into

Table 3 Geometrical parameters of the composite cylindrical lattice shell

Shell height	125 mm
Shell inner diameter	140 mm
Shell thickness	0.4 mm
Unit cell height	127 mm
Unit cell circumferential length	73.3 mm
Stiffener orientation	$\pm 60^\circ$
Stiffener cross-section	6×6 mm^2

Table 4 Comparison of the natural frequencies of SNA-SNA composite lattice cylindrical shells

n	t = 0.4 mm			t = 0.8 mm			t = 1 mm		
	NF-1	NF-2	PM	NF-1	NF-2	PM	NF-1	NF-2	PM
2	2057	2212	2257	2131	1908	1968	2136	1786	1852
3	1654	1421	1536	1662	1457	1543	1663	1418	1478
4	2371	2006	2198	2445	1978	2165	2462	1959	2264
5	2947	2955	3050	3074	2817	2891	3228	2807	3112

* NF-1:Hemmatnezhad *et al*. (2014) - FEM; NF-2: Hemmatnezhad *et al*.(2014) - Analytic; PM: Present Method

Table 5 Comparison of the natural frequency for four values of circumferential mode numbers and different thicknesses of outer skin ($\alpha = 18^{\circ}, L\sin(\alpha)/R_2 = 0.625,\ A_h = 24 \times 24$ mm^2)

n	t = 2 mm			t = 4 mm		
	PM		FEM (ANSYS)	PM		FEM (ANSYS)
	Ave2	Ave11		Ave2	Ave11	
1	126.4258	154.2781	188.1049	176.2207	196.3995	196.0783
2	253.1236	255.4210	206.4152	302.1164	310.2059	216.4567
3	323.4134	348.4814	244.1326	369.9766	391.4711	262.5229
4	368.0047	399.0656	292.2194	398.9260	424.9235	318.6125

* PM: Present Method; Ave2: Average of 2 points; Ave11: Average of 11 points

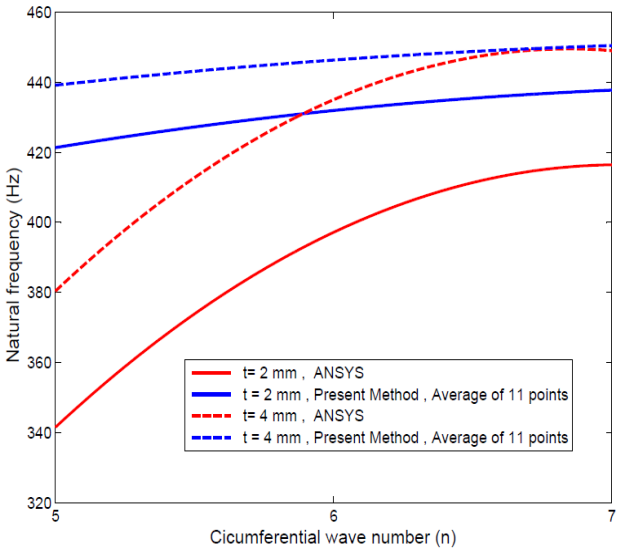

Fig. 9 Variation of the natural frequency respect to the circumferential wave number a SNA–SNA conical lattice shell ($\alpha = 18^{\circ}, L\sin(\alpha)/R_2 = 0.625$, $t = 2, 4$ mm, $A_h = 24 \times 24$ mm^2)

three different meshes in circumferential and axial direction, which satisfies the requirement of convergence. The calculated natural frequencies by FEM are compared with those via present method for a SNA–SNA composite lattice conical shell with outer skin. The natural frequencies via the present method are the average values in two points $x^* = 0.8$ and $x^* = 0.9$ (closer to the large diameter of conical shell) and those computed in eleven points along dimensionless length of conical lattice shell from 0 to 1 with a increment equal 0.1. Table 5 illustrates a comparison of these natural frequencies. The results are given for four circumferential wave numbers from 1 to 4 and two different shell thicknesses. For more illustration, in Fig. 9 the natural frequencies for composite conical lattice shell with the characteristics shown in Table 5 for circumferential wave numbers from 5 to 7 is depicted. The comparison of the resent results suggests that with increasing the circumferential wave number more than six and for thickness of outer skin equal to 4 mm, the natural frequencies via present method and FEM started to converge. As can be seen from this figure, the influence of shell thickness variation on the frequency curve is significant, and the natural frequencies for this case increases by an increment in the shell thickness. This is because of the fact that an increase in the shell thickness increases the stiffness faster than the mass.

Additionally, Table 6 shows a comparison between the natural frequencies of composite conical lattice shell with outer laminated skin via present analytical method and those calculated by FEM Software for seven values of circumferential mode numbers and different boundary conditions. The boundary conditions are SNA–SNA, clamped–clamped (C–C), and clamped–free (C–F). Clearly it would be seen, that the boundary conditions affects the natural frequencies of the composite conical lattice shell. As expected before, the fully clamped composite shell has the highest natural frequencies among the selected boundary conditions. In addition the natural frequencies computed via present method converge for circumferential wave numbers greater than six. However, from the comparison between the two analyses, it can be concluded that the present analytical procedure can be well used for realizing and determining the dynamical behavior of composite lattice conical shells. For more realization, Fig. 10 depicts the mode shapes of vibration of a lattice composite conical

Table 6 Comparison of the natural frequency of composite lattice conical shell for different boundary conditions. ($\alpha = 18^{\circ}$, $L\sin(\alpha)/R_2 = 0.625$, $t = 3$ mm, $A_h = 24 \times 11.4$ mm^2)

n	C − F			SNA − SNA			C − C		
	PM		FEM (ANSYS)	PM		FEM (ANSYS)	PM		FEM (ANSYS)
	Ave2	Ave11		Ave2	Ave11		Ave2	Ave11	
1	193.712	219.763	185.078	208.846	225.438	201.628	226.634	245.328	220.078
2	307.356	324.937	211.483	325.618	337.445	215.656	369.634	384.328	258.078
3	363.663	379.105	227.532	384.913	406.123	234.952	419.634	442.328	271.078
4	381.467	404.312	258.010	409.420	432.612	273.325	435.634	457.328	298.078
5	401.155	421.868	297.267	420.8124	444.224	319.956	455.635	474.328	344.851
6	414.810	436.783	344.900	426.010	450.240	361.511	457.635	481.329	387.318
7	417.457	442.575	371.279	428.609	453.744	374.181	460.635	485.329	397.778

* PM: Present Method; Ave2: Average of 2 points; Ave11: Average of 11 points

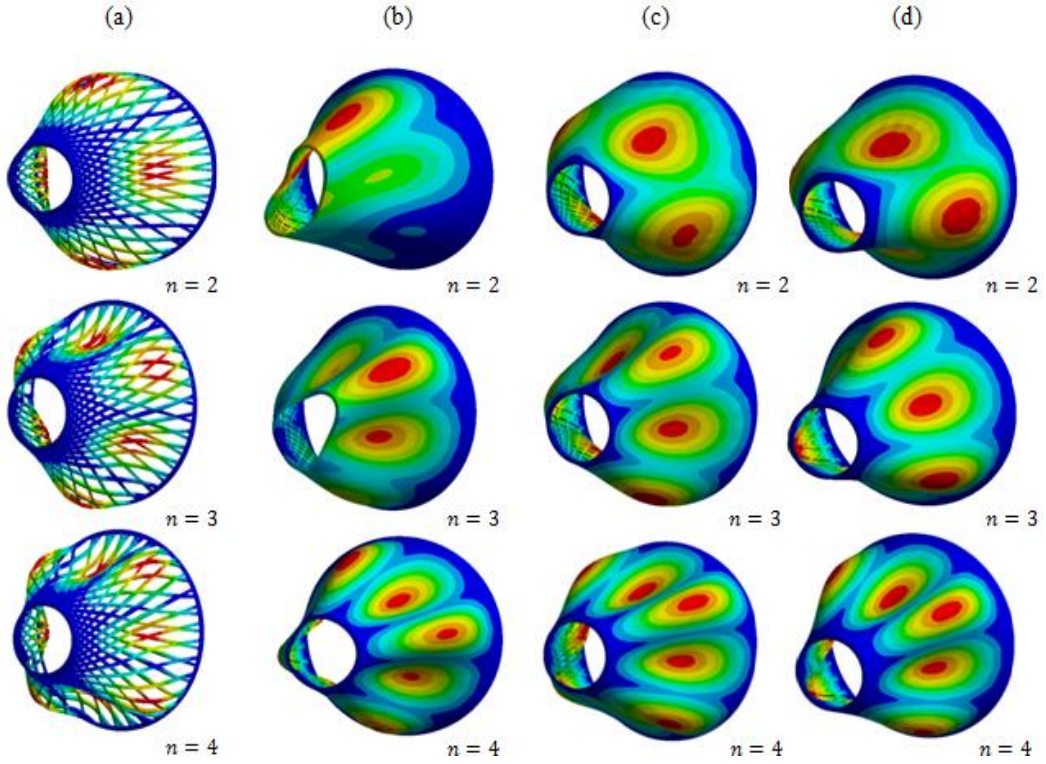

Fig. 10 Mode shapes associated with (a) SNA–SNA (Skinless); (b) C-F; (c) SNA–SNA; and (d) C-C composite lattice conical shell ($\alpha = 18^{\circ}, L\sin(\alpha)/R_2 = 0.625$)

shell associated with different boundary conditions. The shell is considered with and without outer laminated skin.

References

Ansari, R. and Darvizeh, M. (2008), "Prediction of dynamic behavior of FGM shells under arbitrary boundary conditions", *Compos. Struct.*, **85**(4), 284-292.

Ansari, R. and Torabi, J. (2016), "Numerical study on the buckling and vibration of functionally graded carbon nanotube-reinforced composite conical shells under axial loading", *Compos. Part B: Eng.*, **95**, 196-208.

Bakshi, K. and Chakravorty, D. (2013), "Relative static and dynamic performances of composite conoidal shell roofs", *Steel Compos. Struct., Int. J.*, **15**(4), 379-397.

Buragohain, M. and Velmurugan, R. (2011), "Study of filament wound grid-stiffened composite cylindrical structures", **93**(2), 1031-1038.

Chang, C.H. (1981), "Vibrations of conical shells", *Shock Vib. Digest.*, **13**(6), 9-17.

Civalek, O. (2006a), "Free vibration analysis of composite conical shells using the discrete singular convolution algorithm", *Steel Compos. Struct., Int. J.*, **6**(4), 353-366.

Civalek, O. (2006b) "An efficient method for free vibration analysis of rotating truncated conical shells", *Int. J. Press. Vess. Pip.*, **83**(1), 1-12.

Civalek, O. (2007), "Linear vibration analysis of isotropic conical shells by discrete singular convolution (DSC)", *Int. J. Struct. Eng. Mech.*, **25**(1), 127-130.

Civalek, O. (2008), "Vibration analysis of conical panels using the

method of discrete singular convolution", *Commun. Numer. Methods Eng.*, **24**(3), 169-181.
Civalek, O. (2013), "Vibration analysis of laminated composite conical shells by the method of discrete singular convolution based on the shear deformation theory", *Compos.*: *Part B*, **45**(1), 1001-1009.
Darilmaz, K. (2012), "Stiffened orthotropic corner supported hypar shells: Effect of stiffener location, rise/span ratio and fiber orientaton on vibration behavior", *Steel Compos. Struct., Int. J.*, **12**(4), 275-289.
Garnet, H. and Kempner, J. (1960), "Axisymmetric free vibrations of conical shells", *J. Appl. Mech.*, **31**(3), 458-466.
Golfman, Y. (2007), "Dynamic stability of the lattice structures in the manufacturing of carbon fiber epoxy/composites including the influence of damping properties", *J. Adv. Mater.* (*Special Ed.*), **3**, 11-20.
Gürdal, Z. and Gendron, G. (1993), "Optimal design of geodesically stiffened composite cylindrical shells", *Compos. Eng.*, **3**(12), 1131-1147.
Hemmatnezhad, M., Rahimi, G.H. and Ansari, R. (2014), "On the free vibrations of grid-stiffened composite cylindrical shells", *Acta Mech.*, **225**(2), 609-623.
Irie, T., Yamada, G. and Kaneko, Y. (1982), "Free vibration of a conical shell with variable thickness", *J. Sound Vib.*, **82**(1), 83-94.
Irie, T., Yamada, G. and Tanaka, K. (1984), "Natural frequencies of truncated conical shells", *J. Sound Vib.*, **92**(3), 447-453.
Kadoli, R. and Ganesan, N. (2003), "Free vibration and buckling analysis of composite cylindrical shells conveying hot fluid", *Compos. Struct.*, **60**(1), 19-32 **.**
Kidane, S., Li, G., Helms, J., Pang, S. and Woldesenbet, E. (2003), "Buckling load analysis of grid stiffened composite cylinders", *Compos.*: *Part B*, **34**(1), 1-9.
Kim, T.D. (1999), "Fabrication and testing of composite isogrid stiffened cylinder", *Compos. Struct.*, **45**(1), 1-6.
Kim, T.D. (2000), "Fabrication and testing of thin isogrid composite stiffened panel", *Compos. Struct.*, **49**(1), 21-45.
Liang, W., He, Y., Yang, L.L. and Sha, L. (2011), "The buckling and dynamic analysis of composite grid stiffened structure", *Appl. Mech. Mater.*, **52**, 1794-1799.
Liew, K.M. and Lim, C.W. (1995), "Vibratory characteristics of cantilevered rectangular shallow shells of variable thickness", *AIAA J.*, **32**(2), 387-396.
Liew, K.M., Lim, M.K., Lim, C.W., Li D.B. and Zhang, Y.R. (1995), "Effects of initial twist and thickness variation on the vibration behaviour of shallow conical shells", *J. Sound Vib.*, **180**(2), 271-296.
Liew, K.M., Lim, C.W. and Kitipornchai, S. (1997) "Vibration of shallow shells: a review with bibliography", *J. Appl. Mech. Rev.*, **50**, 431-444.
Liew, K.M., Ng, T.Y. and Zhao, X. (2005), "Free vibration analysis of conical shells via the element-free kp-Ritz method", *J. Sound Vib.*, **281**(3), 627-645.
Lim, C.W. and Liew, K.M. (1995), "Vibratory behavior of shallow conical shells by a global Ritz formulation", *Eng. Struct.*, **17**(1), 63-70.
Lim, C.W., Liew, K.M. and Kitipornchai, S. (1998), "Vibration of cantilevered laminated composite shallow conical shells", *Int. J. Solids Struct.*, **35**(15), 1695-1707.
Lopatin, A.V., Morozov, E.V. and Shatov, A.V. (2015), "Fundamental frequency of a cantilever composite filament-wound anisogrid lattice cylindrical shell", *Compos. Struct.*, **133**, 564-575.
Lopatin, A.V., Morozov, E.V. and Shatov, A.V. (2016), "An analytical expression for fundamental frequency of the composite lattice cylindrical shell with clamped edges", *Compos. Struct.*, **141**, 232-239.
Morozov, E.V., Lopatin, A.V. and Nesterov, V.A. (2011), "Buckling analysis and design of anisogrid composite lattice conical shells", *Compos. Struct.*, **93**(12), 3150-3162.
Qatu, M.S. (2004), *Vibration of Laminated Shells and Plates*, Elsevier, Academic Press, Amsterdam, Netherlands.
Saunders, H., Wisniewski, E.J. and Pasley, P.R. (1960), "Vibration of conical shells", *J. Acoust. Soc. Am.*, **32**(6), 765-772.
Shi, S., Sun, Z., Ren, M., Chen, H. and Hu, X. (2013), "Buckling resistance of grid- stiffened carbon-fiber thin-shell structures", *Compos.*: *Part B*, **45**, 888-896.
Shu, C. (1996), "Free vibration analysis of composite laminated conical shells by generalized differential quadrature", *J. Sound Vib.*, **194**(4), 587-604.
Sivadas, K.R. and Ganesan, N. (1992), "Vibration analysis of thick composite clamped conical shells with variable thickness", *J. Sound Vib.*, **152**(1), 27-37.
Siu, C.C. and Bert, C.W. (1970), "Free vibrational analysis of sandwich conical shells with free edges", *J. Acoust. Soc. Am.*, **47**(3B), 943-955.
Slinchenko, D. and Verijenko, V.E. (2001), "Sructural analysis of composite lattice shells of revolution on the basis of smearing stiffness", *Compos. Struct.*, **54**(2), 341-348.
Sofiyev, A.H. and Karaca, Z. (2009), "The vibration and stability of laminated non homogeneous orthotropic conical shells subjected to external pressure", *Eur. J. Mech. – A/Solids*, **28**(2), 317-328.
Sofiyev, A.H. and Kuruoglu, N. (2011), "Natural frequency of laminated orthotropic shells with different boundary conditions and resting on the Pasternak type elastic foundation", *Compos. Part B*: *Eng.*, **42**(6), 1562-1570.
Sofiyev, A.H., Omurtag, M. and Schnack, E. (2009), "The vibration and stability of orthotropic conical shells with non-homogeneous material properties under a hydrostatic pressure", *J. Sound Vib.*, **319**(3), 963-983.
Tong, L. (1993a), "Free vibration of orthotropic conical shells", *Int. J. Eng. Sci.*, **31**(5), 719-733.
Tong, L. (1993b), "Free vibration of composite laminated conical shells", *Int. J. Mech. Sci.*, **35**(1), 47-61.
Tong, L. (1994), "Free vibration of laminated conical shells including transverse shear deformation", *Int. J. Solids Struct.*, **31**(4), 443-456.
Totaro, G. (2011), "Multilevel optimization of anisogrid lattice structures for aerospace", Ph.D. Thesis; Delft University of Technology, Delft, Netherlands.
Totaro, G. (2012), "Local buckling modelling of isogrid and anisogrid lattice cylindrical shells with triangular cells", *Compos. Struct.*, **94**(2), 446-452.
Totaro, G. (2013a), "Local buckling modelling of isogrid and anisogrid lattice cylindrical shells with hexagonal cells", *Compos. Struct.*, **94**(2), 403-410.
Totaro, G. (2013b), "Local buckling modelling of isogrid and anisogrid lattice cylindrical shells with hexagonal cells", *Compos. Struct.*, **95**, 403-410.
Totaro, G. and De Nicola, F. (2012), "Recent advance on design and manufacturing of composite anisogrid structures for space launchers", *Acta Astronaut.*, **81**(2), 570-577.
Totaro, G. and Gürdal, Z. (2005), "Optimal design of composite lattice structures for aerospace application", *Proceedings of European Conference for Aerospace Sciences* (*EUCASS*), Moscow, Russia, July.
Totaro, G. and Gürdal, Z. (2009), "Optimal design of composite lattice shell structures for aerospace applications", *Aerosp. Sci. Technol.*, **13**(4), 157-164.
Vasiliev, V.V. and Rasin, A.F. (2006), "Anisogrid composite lattice structures for spacecraft and aircraft applications", *Compos. Struct.*, **76**(1), 182-189.
Vasiliev, V.V., Barynin, V.A. and Rasin, A.F. (2001), "Anisogrid

lattice structures-survey of development and application", *Compos. Struct*., **54**(2), 361-370.
Wodesenbet, E., Kidane, S. and Pang, S. (2003), "Optimization for buckling loads of grid stiffened composite panels", *Compos. Struct*., **60**(2), 159-169.
Yang, C.C. (1974), "On vibrations of orthotropic conical shells", *J. Sound Vib*., **34**(4), 552-555.

CC

Appendix A

In employment of the differentiating a Fourier series, it should be particularly attentive to border values at the ends. For example, the end values of the functions represented by sine series are forced to be zero, but using Stokes' transformation, the end values of the sine series are released by being defined separately. Consider a function $f(x)$ represented by a Fourier sine series in the open range $0 < x < L$ and by values f_0 and f_L at the end points as

$$f(x) = \sum_{n=1}^{\infty} a_n \sin(\frac{n\pi x}{L}), \qquad 0 < x < L,$$
$$f(0) = f_0 \quad , f(L) = f_L,$$

Since in doubt that the derivative $f'(x)$ can be represented by term-by-term differentiation of the sine series, the derivative is instead represented by an independent cosine series as following form

$$f'(x) = b_0 + \sum_{n=1}^{\infty} b_n \cos\frac{n\pi x}{L}$$

Stokes' transformation consists of integrating by parts in the basic definitions of the coefficients to obtain the relationship between b_n and a_n as follows

$$\begin{aligned} b_n &= \frac{2}{L}\int_0^L f'(x)\cos\frac{n\pi x}{L}dx \\ &= \frac{2}{L}\left[f(x)\cos\frac{n\pi x}{L}\right]_0^L + \frac{2n\pi}{L^2}\int_0^L f(x)\sin\frac{n\pi x}{L}dx \\ &= \frac{2}{L}\left[(-1)^n f_L - f_0\right] + \frac{n\pi x}{L}a_n, \end{aligned}$$

The similar care must be taken when finding the correct sine series corresponding to $f''(x)$. Therefore, the complete set of derivative formulas for the sine series can be written as

$$\begin{cases} f(x) = \sum_{n=1}^{\infty} a_n \sin(\frac{n\pi x}{L}), 0 < x < L \\ f(0) = f_0 \quad , \quad f(L) = f_L, \end{cases}$$

$$f'(x) = \frac{f_L - f_0}{2} - \sum_{n=1}^{\infty}\left[\frac{2}{L}\left\{f_0 - (-1)^n f_L\right\} - \frac{\pi}{L}na_n\right]\cos(\frac{n\pi x}{L}), 0 \le x \le L$$

$$\begin{cases} f''(x) = \frac{\pi}{L}\sum_{n=1}^{\infty} n\left[\frac{2}{L}\left\{f_0 - (-1)^n f_L\right\} - \frac{\pi}{L}na_n\right]\sin(\frac{n\pi x}{L}), 0 < x < L \\ f''(0) = f_0'' \quad , \quad f''(L) = f_L'', \end{cases}$$

Similar transformation formulas must be used to obtain the correct form of the successive derivatives of the cosine series. These formulae are used for the derivatives of displacement functions in the solution procedure of the present analysis. Some of the derivatives of displacement functions are given in the following

$$u(x,\theta,t) = \left(U_{0n} + \sum_{m=1}^{\infty}\sum_{n=1}^{\infty} U_{mn}\cos(\lambda x)\right) \cos(\eta\theta)\cos(\omega t), 0 \le x \le x_0,$$

$$u_{,x} = -\left(\frac{\pi}{x_0}\right)\sum_{m=1}^{\infty}\sum_{n=1}^{\infty} mU_{mn}\sin(\lambda x) \cos(\eta\theta)\cos(\omega t), \quad 0 < x < x_0,$$

$$u_{,x}(0,\theta) = -\left(\frac{\pi^2}{2x_0}\right)\bar{u}_0\cos(\eta\theta),$$

$$u_{,x}(x_0,\theta) = -\left(\frac{\pi^2}{2x_0}\right)\bar{u}_{x_0}\cos(\eta\theta),$$

$$u_{,xx} = -\left(\frac{\pi}{x_0}\right)^2\left(\frac{\bar{u}_0 + \bar{u}_{x_0}}{2} + \sum_{m=1}^{\infty}\sum_{n=1}^{\infty}\left\{\bar{u}_0 + \bar{u}_{x_0}(-1)^m - m^2U_{mn}\right\}\cos(\lambda x)\right) \cos(\eta\theta)\cos(\omega t), 0 \le x \le x_0,$$

$$v(x,\theta,t) = \sum_{m=1}^{\infty}\sum_{n=1}^{\infty} V_{mn}\sin(\lambda x)\sin(\eta\theta)\cos(\omega t) \qquad 0 < x < x_0,$$

$$v(0,\theta) = -\left(\frac{\pi}{2}\right)v_0\sin(\eta\theta),$$

$$v(x_0,\theta) = \left(\frac{\pi}{2}\right)v_{x_0}\sin(\eta\theta),$$

$$v_{,x} = \left(\frac{\pi}{x_0}\right)\left(\frac{v_0 + v_{x_0}}{2} + \sum_{m=1}^{\infty}\sum_{n=1}^{\infty}\left\{v_0 + v_{x_0}(-1)^m + mV_{mn}\right\}\cos(\lambda x)\right) \sin(\eta\theta)\cos(\omega t), 0 \le x \le x_0,$$

$$v_{,xx} = -\left(\frac{\pi}{x_0}\right)^2\left(\sum_{m=1}^{\infty}\sum_{n=1}^{\infty}\left\{v_0 m + v_{x_0}m(-1)^m + m^2V_{mn}\right\}\sin(\lambda x)\right) \sin(\eta\theta)\cos(\omega t), \quad 0 < x < x_0,$$

$$w(x,\theta,t) = \sum_{m=1}^{\infty}\sum_{n=1}^{\infty} W_{mn}\sin(\lambda x) \cos(\eta\theta)\cos(\omega t),$$

$$w(0,\theta) = -\left(\frac{\pi}{2}\right)w_0\cos(\eta\theta),$$

$$w(x_0,\theta) = \left(\frac{\pi}{2}\right)w_{x_0}\cos(\eta\theta),$$

The successive derivatives with respect to θ and t are simply achieved. For example, the successive derivatives of $u(x, \theta, t)$ with respect to θ are as follows

$$w_{,x} = \left(\frac{\pi}{x_0}\right)\left(\frac{w_0 + w_{x_0}}{2} + \sum_{m=1}^{\infty}\sum_{n=1}^{\infty}\left\{w_0 + w_{x_0}(-1)^m + mW_{mn}\right\}\cos(\lambda x)\right),$$
$$\cos(\eta\theta)\cos(\omega t), 0 \le x \le x_0,$$

$$w_{,xx} = -\left(\frac{\pi}{x_0}\right)^2\left(\sum_{m=1}^{\infty}\sum_{n=1}^{\infty}\left\{w_0 m + w_{x_0} m(-1)^m + m^2 W_{mn}\right\}\sin(\lambda x)\right)$$
$$\cos(\eta\theta)\cos(\omega t), \quad 0 < x < x_0,$$

$$w_{,xx}(0,\theta) = -\left(\frac{\pi^3}{2x_0^2}\right)\overline{\overline{w}}_0\cos(\eta\theta),$$

$$w_{,xx}(x_0,\theta) = \left(\frac{\pi^3}{2x_0^2}\right)\overline{\overline{w}}_{x_0}\cos(\eta\theta),$$

$$\psi_x(x,\theta,t) = (\Psi_{0n1} + \sum_{m=1}^{\infty}\sum_{n=1}^{\infty}\Psi^1_{mn}\cos(\lambda x))$$
$$\cos(\eta\theta)\cos(\omega t), \quad 0 \le x \le x_0,$$

$$\psi_{x,x} = -\left(\frac{\pi}{x_0}\right)\sum_{m=1}^{\infty}\sum_{n=1}^{\infty}m\Psi^1_{mn}\sin(\lambda x)$$
$$\cos(\eta\theta)\cos(\omega t), \quad 0 < x < x_0,$$

$$\psi_{x,x}(0,\theta) = -\left(\frac{\pi^2}{2x_0}\right)\overline{\psi}_0\cos(\eta\theta),$$

$$\psi_{x,x}(x_0,\theta) = -\left(\frac{\pi^2}{2x_0}\right)\overline{\psi}_{x_0}\cos(\eta\theta),$$

$$\psi_{x,xx} = \left(\frac{\pi}{x_0}\right)^2\left(\frac{\overline{\psi}_0 + \overline{\psi}_{x_0}}{2} + \sum_{m=1}^{\infty}\sum_{n=1}^{\infty}\left\{\overline{\psi}_0 + \overline{\psi}_{x_0}(-1)^m - m^2\Psi^1_{mn}\right\}\cos(\lambda x)\right)$$
$$\cos(\eta\theta)\cos(\omega t), \quad 0 \le x \le x_0,$$

$$\psi_\theta(x,\theta,t) = \sum_{m=1}^{\infty}\sum_{n=1}^{\infty}\Psi^2_{mn}\sin(\lambda x)\sin(\eta\theta)$$
$$\cos(\omega t), \quad 0 < x < x_0,$$

$$\psi_\theta(0,\theta) = -\left(\frac{\pi}{2}\right)\psi_\theta^0\sin(\eta\theta),$$

$$\psi_\theta(x_0,\theta) = \left(\frac{\pi}{2}\right)\psi_\theta^{x_0}\sin(\eta\theta),$$

$$\psi_{\theta,x} = \left(\frac{\pi}{x_0}\right)\left(\frac{\psi_\theta^0 + \psi_\theta^{x_0}}{2} + \sum_{m=1}^{\infty}\sum_{n=1}^{\infty}\left\{\psi_\theta^0 + \psi_\theta^{x_0}(-1)^m + m\Psi^2_{mn}\right\}\cos(\lambda x)\right)$$
$$\sin(\eta\theta)\cos(\omega t), 0 \le x \le x_0,$$

$$\psi_{\theta,xx} = -\left(\frac{\pi}{x_0}\right)^2$$
$$\left(\sum_{m=1}^{\infty}\sum_{n=1}^{\infty}\left\{\psi_\theta^0 m + \psi_\theta^{x_0} m(-1)^m + m^2\Psi^2_{mn}\right\}\right.$$
$$\left.\sin(\lambda x)\right)\sin(\eta\theta)\cos(\omega t), \quad 0 < x < x_0,$$